PHYSICAL REVIEW C
NUCLEAR PHYSICS

THIRD SERIES, VOLUME 29, NUMBER 5 MAY 1984

Fragment mass, energy, and angular distributions for the ^{12}C(^{4}He, heavy ion) reaction between 49 and 159 MeV

A. Gökmen,* H. Breuer, A. C. Mignerey, and B. G. Glagola†
Departments of Physics and Chemistry, University of Maryland, College Park, Maryland 20742

K. Kwiatkowski and V. E. Viola, Jr.
Department of Chemistry and Indiana University Cyclotron Facility, Indiana University, Bloomington, Indiana 47405

(Received 22 June 1983)

Inclusive mass, energy, and angular distributions of all fragments with $A \geq 6$ have been measured for alpha-particle-induced reactions on ^{12}C at five energies between 49 and 159 MeV. From these data the evolution of the dominant reaction mechanisms with energy is characterized. Based on analysis of the mean value of the mass distribution, it appears that linear momentum transfer from projectile to target initially increases with beam energy and reaches a maximum at about 30—40 MeV/nucleon. The low-energy data are consistent with compound nucleus formation and simple transfer processes. At higher energies the growth of forward-peaked angular distributions, continuum energy spectra, and the disappearance of two-body states demonstrate the increasing importance of nucleon-nucleon collisions and multibody breakup mechanisms as the velocity of the projectile exceeds the Fermi velocity. The observed total reaction cross section decreases with increasing bombarding energy. Inclusion of these new data into the excitation functions for $6 \leq A \leq 11$, which are required for nucleosynthesis calculations relevant to the origin of the elements Li, Be, and B, does not significantly alter conclusions based on previously available data.

I. INTRODUCTION

In the last two decades nuclear reaction mechanism studies have focused on two extreme ranges of projectile energies: (1) the low-energy regime from the Coulomb barrier to ~20 MeV/nucleon and (2) the high-energy region above about 100 MeV/nucleon. In the intermediate-energy region it has been suggested that new reaction mechanisms may appear when the projectile velocity exceeds both the velocity of sound in nuclear matter and the Fermi velocity.[1] Certainly one expects to observe the transition from mean-field effects at low energies to nucleon-nucleon collision effects at high energies.

Until very recently the alpha particle has been the heaviest complex projectile available in this energy range. Although macroscopic coherent effects are expected to be accentuated for heavier ions, it is essential that the basic interaction features for a relatively simple projectile such as the alpha particle be understood in order to recognize and identify more exotic phenomena.

The primary purpose of this research has been to investigate the salient mechanisms which describe the total reaction cross section, σ_R, for alpha-particle-induced reactions on light-target nuclei (^{12}C, ^{14}N, and ^{16}O) in the transition-energy range from 10 to 40 MeV/nucleon. In previous studies of similar systems, most of the effort has been directed toward the measurement of light-ion spectra.[2–5] In addition, gamma rays from low-lying states of heavy fragments[6,7] have been used to gain information on a few bound states; however, these constitute only a small part of the reaction cross section. Some data also exist on the mass and charge distributions of heavy fragments from the ^{4}He+^{27}Al reaction.[7]

The experimental focus of the present study has been to measure the complete mass, energy, and angular distributions for all reaction products with $A \geq 6$, identifying product masses unambiguously. Because the targetlike residual nuclei represent the net consequences of both the collision and decay stages of the total interaction, such studies provide a different perspective on the deposition of energy and transfer of linear momentum in a given reaction than do inclusive light-charged particle measurements. Moreover, one can estimate the relative importance of the various reaction channels that comprise the total cross section. For example, from the energy and angular spectra of fragments with $A \geq 6$, both low-lying two-body and multibody (≥ 3) final states can be identified and for the former, it is possible to determine whether these fragments originate from compound nucleus formation or direct interactions. Interpretation of the data presented in this paper will focus on the qualitative understanding of the predominant underlying reaction mechanisms. In an accompanying paper a comparison of the data with theoretical predictions of an intranuclear cascade-statistical decay calculation will provide a more quantitative evaluation of the data.[8]

A related problem of current interest is the measurement of total reaction cross sections for complex projectiles in the intermediate energy region.[9,10] The experimental total reaction cross sections for low-energy collisions at energies above the resonance region can be described semiclassically.[11–13] As the beam energy increases above about 20 MeV/nucleon, σ_R decreases from its maximum value to a minimum in the energy region ($150 \leq E/A \leq 300$ MeV/nucleon). The decrease in σ_R with beam energy has been ascribed to a transparency of the target nucleus[9] or a decrease in the geometric cross section of the interacting system.[14] The data obtained in this work provide an independent check of the dependence of σ_R on beam energy, which can be used for comparison with results derived from elastic scattering and beam attenuation techniques.

Finally, alpha-particle-induced reactions on ^{12}C, ^{14}N, and ^{16}O target nuclei have astrophysical importance for Li, Be, and B nucleosynthesis. Among various models, the interaction of galactic cosmic rays (GCR) with the interstellar medium has met with the greatest success for explaining ^{6}Li, ^{9}Be, ^{10}B, and ^{11}B production.[15] The excitation functions for fragments with $6 \leq A \leq 11$ from the ^{4}He+^{12}C reaction at beam energies from 49 to 159 MeV, combined with recent data from the ^{4}He+^{14}N and ^{4}He+^{16}O reactions[16] at beam energies from 50 to 80 MeV, provide a more complete set of data with which the validity of the proposed models of LiBeB synthesis can be assessed.

II. EXPERIMENTAL PROCEDURES AND DATA ANALYSIS

A. Experimental apparatus

The primary experimental objective of this study was to determine the mass, energy, and angular distributions of all reaction products with $A \geq 6$ as a function of beam energy for alpha-particle-induced reactions on a ^{12}C target. The experiments were carried out at the University of Maryland Cyclotron using 49.0-, 61.0-, 80.1-, 121.0-, and 159.3-MeV alpha-particle beams to bombard ^{12}C targets with thicknesses of 50–100 μg/cm^2. The beam current ranged from about 20 nA for forward angle measurements to 300 nA for backward angles. Absolute cross sections were calculated from the known target thickness, count rate, detector geometry, and integrated beam current.

The principal experimental technique in our measurements was time-of-flight (TOF) mass identification. The TOF detector telescope consisted of four detectors. A channel-plate fast-timing device[17,18] (CPFTD) served as the first (start) element in the telescope, followed by a 45-μm surface-barrier transmission detector 23 cm from the CPFTD foil. This detector was used simultaneously as the second (stop) timing detector, as an energy E detector for stopping fragments, and as a ΔE detector for transmitted ions. A second surface barrier detector of thickness 400 μm served as an energy detector for all stopping particles which penetrated the first ΔE element. A third surface barrier detector (4 mm Li-drifted Si) was used in the telescope to veto energetic light ions (H,He). In these experiments the timing uncertainty, Δt, was not measured directly; however, an upper limit of 130 psec was estimated from the mass resolution of the reaction products.

B. Data reduction

Detector energy calibrations were performed with ^{148}Gd and ^{241}Am alpha-particle sources. The energies of well-defined two-body states observed in the data usually agreed to within 0.3 MeV of the kinematically expected value. A small observed energy shift was attributed mainly to energy loss of the products in the target material and the channel-plate carbon foil. In the ^{4}He+^{12}C reactions only a small fraction of the product ions were stopped in the carbon foil (e.g., for ^{15}N only ions with an energy <0.1 MeV are stopped in a 50-μg/cm^2 thick carbon foil). Therefore, no corrections have been made for these effects.

Transformation of the fragment time-of-flight T and energy E data into masses M followed two approaches. The first (applied to the 80-MeV data) considered a mass transformation function of the form

$$M = a + b(c + dE)(T + t_0 + eE + fE^2 + gM + hM^2)^2 \, , \quad (1)$$

where a to h and t_0 are parameters which were optimized to yield straight mass lines over the entire mass-versus-energy spectrum.[16] The parameters c and d are corrections for the nonlinearities in energy, t_0 is a time offset, and e, f, g, and h are parameters to make corrections for the nonlinearities in the timing system. The disadvantage of this method is that it is still not completely successful in straightening the mass lines at the lowest energies (e.g., $0.5 \leq E \leq 2$ MeV) for the heaviest products. The result of transforming the 80-MeV data is shown in Fig. 1 for fragments with energies ≥ 2 MeV. This spectrum is typical of the energy-gated mass spectra obtained at all bombarding energies. For fragments with $E \geq 2$ MeV a mass resolution of $\sim$0.4–0.5 u was generally obtained; this de-

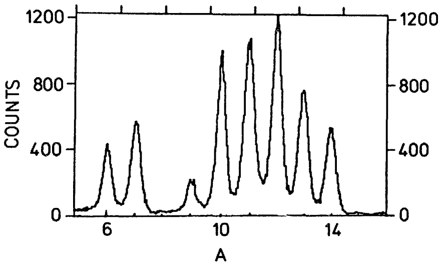

FIG. 1. Mass spectrum for the 80-MeV ^{4}He+^{12}C reaction observed at a laboratory angle of 30 deg. All events with an energy > 2 MeV are included in the plot.

teriorated to a value of ~1 u at the lowest fragment energies (~0.5 MeV).

For the low-energy 80-MeV data and the data at other energies a second approach has been used. This method defined two-dimensional nonlinear gates around the mass lines as defined by a two-dimensional E vs Et^2 contour.[19] The energy spectra could then be projected out for each mass and integrated to yield cross section information. Charge identification was determined by standard ΔE-E techniques for all fragments which penetrated the first silicon detector. Due to the fact that most of the yield in these reactions is concentrated at comparatively low energies, only a small fraction of the total cross section of ions with $Z>3$ could be identified according to charge. Hence, the charge information has only been used for channel-plate efficiency corrections (Sec. II C).

The electronic low-energy threshold was 0.5 MeV for all but the 121-MeV ^{4}He+^{12}C experiment, for which it was about 2 MeV. To correct each isobaric yield for the unmeasured, low-energy portion of the fragment energy spectrum, the average number of counts per bin just above the low energy cutoff was extrapolated to zero MeV, assuming a constant value of counts per bin for the missing energies. This was then integrated to estimate the total yield in that unmeasured region. A 50% error in the extrapolated low-energy yield was assumed to account for uncertainties in the undefined region of the spectrum and for heavy ions stopped in the target material. This was then added in quadrature with the other errors (i.e., uncertainty in target thickness, flight path, angle measurement, beam-current integrator, errors from CPFTD inefficiency corrections, and statistical errors) to determine the final error.

To estimate the portion of the angular distribution not covered in these experiments, the differential cross section, $d\sigma/d\theta$, has been extrapolated linearly from 10 to 0 deg and from the most backward measured angle to the kinematic limit (or 180°) at backward angles.

C. CPFTD efficiency

In order to determine fragment cross sections in these experiments, it is necessary to determine the efficiency of the CPFTD. The CPFTD detects secondary electrons emitted from a 30-μg/cm^2 carbon foil when a given fragment passes through it. Thus, the efficiency of the device depends upon (i) the probability for electron production when the ion to be detected interacts with the carbon foil and (ii) the probability for electron detection by the channel-plate devices. The former probability is assumed to be directly proportional to the stopping power of heavy ions in matter. The latter is mainly determined by the active area of the channel plates and the constant fraction timing discriminator threshold. Assuming this latter probability is constant during a run, one can predict that the efficiency of the CPFTD will be a function of the stopping powers of the heavy ions,[20] as given by the relation

$$n_e \propto \frac{dE}{dx} \propto \frac{MZ^2}{E}\,, \tag{2}$$

where n_e is the number of electrons produced in the carbon foil of the CPFTD, dE/dx is the stopping power of the heavy ion in carbon, and M, Z, and E are the mass, charge, and energy of the heavy ion.

Assuming a Poisson distribution function for electron production in the foil, one can express the particle detection efficiency as

$$P(M,Z,E)=1-\exp\left[-C\frac{dE}{dx}(M,Z,E)\right]\,, \tag{3}$$

where C is a constant determined experimentally for the efficiency P, of detecting an ion with mass M and charge Z at a particular energy E.

The CPFTD efficiencies can be determined experimentally for ions which penetrate the ΔE detector and stop in the E detector. Comparison of the count rate for events producing a valid TOF start-stop signal with those producing a ΔE-E signal (100 percent efficient) yields the efficiency directly. The CPFTD efficiency for detecting various heavy ions in the 80-MeV ^{4}He+^{12}C experiment at 18 deg is shown in Fig. 2. The points and binomial distribution error bars correspond to experimental values; the solid lines are the CPFTD efficiencies calculated using Eq. (3) with a single value of the constant C which best fits the data.

Since the calculated CPFTD efficiencies are successful in reproducing the experimental values for ions $6\leq A\leq 10$ over a broad range of energies, the efficiencies for each ion have been calculated using Eq. (3) and the corresponding ΔE-E data at all beam energies and for each angle measured in these experiments. The energy spectra of ions $A\leq 11$ were then corrected using the calculated efficiencies. The correction to the energy-integrated differential cross sections for $A=6$ and 7 from 121 and 159 MeV experiments are as much as 50 percent for very energetic fragments. The efficiencies approach 100 percent at lower beam energies. The calculated CPFTD efficiencies for ions $A>11$ are greater than 90% in the energy region of highest cross section, and no corrections have been made for these ions.

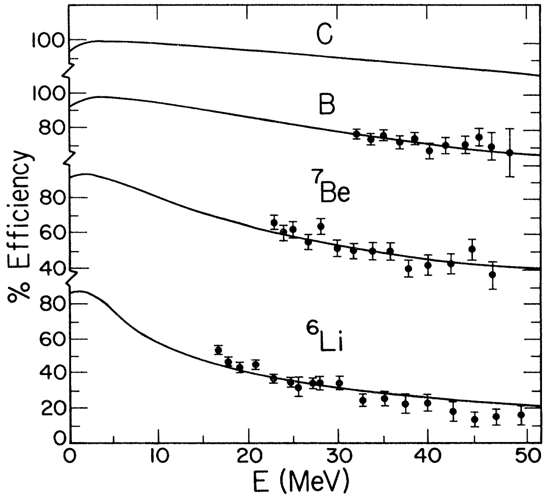

FIG. 2. CPFTD efficiencies as a function of fragment energy for the 80-MeV ^{4}He+^{12}C experiment. Lines are calculated with Eq. (3).

III. EXPERIMENTAL RESULTS

In this section the systematic properties of the energy spectra, angular distributions, mass distributions, and reaction cross sections of heavy fragments are examined. The emphasis of this analysis is directed toward deriving a qualitative overview of the salient reaction mechanisms. In an accompanying paper a more detailed comparison with an intranuclear cascade-statistical decay model is presented.[8]

A. Energy spectra

Among the many energy spectra of reaction products with $A \geq 6$ obtained in these studies only a few representative examples which summarize the most pronounced features of the reactions over the entire mass and energy range will be present here. The energy spectra of fragments with masses $A=7$, 9, 11, 13, and 15 from the 49-MeV reaction at 18 and 40 deg and from the 159-MeV reaction at 20 and 50 deg are compared in Figs. 3(a) and (b), respectively. In Fig. 4 spectra of $A=12$ fragments at various laboratory angles are shown for the 80-MeV bombardment. An important feature of the 49- and 159-MeV energy spectra is the predominance of a broad distribution of fragment energies. The fragment energy spectra from the 49-MeV reaction also exhibit well-defined two-body states which result either from transfer reactions or from binary breakup of the composite system into discrete fragment states. The continuum of events below the discrete states presumably reflect more complex target-projectile interactions involving a wide range of energy deposition. With the many possible combinations of exit channels and associated energy states, a structureless and broad energy distribution results.

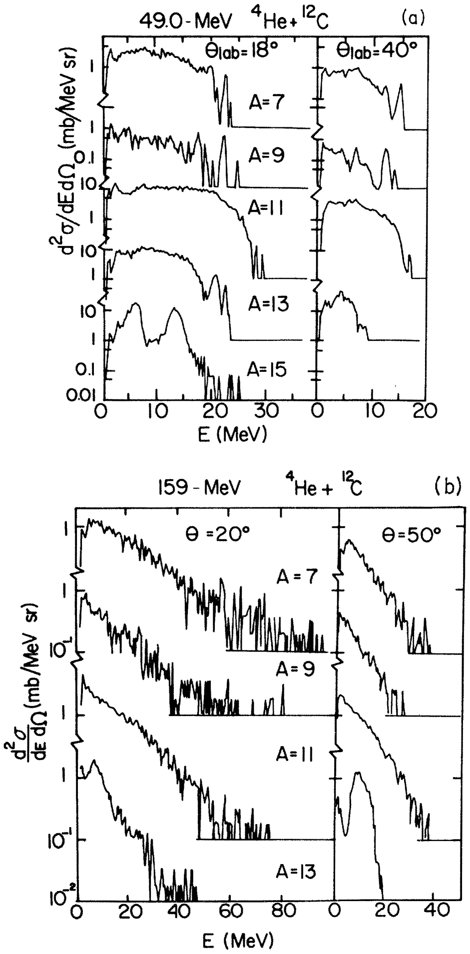

FIG. 3. (a) Energy spectra of fragments with $A=7$, 9, 11, 13, and 15 from the 49-MeV ^{4}He+^{12}C experiment at laboratory angles of 18 and 40 deg; (b) energy spectra of fragments with $A=7$, 9, 11, and 13 from the 159-MeV ^{4}He+^{12}C experiment at laboratory angles of 20 and 50 deg.

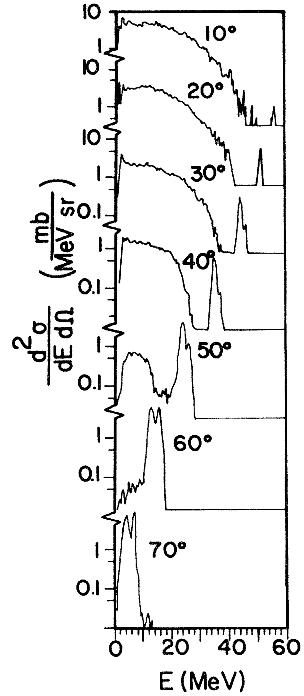

FIG. 4. Energy spectra of $A=12$ fragments as a function of angle for the 80-MeV ^{4}He+^{12}C reaction.

The energy spectra for $A=15$ fragments in Fig. 3(a) represent the combined results for two-body states from the ^{12}C(α,n) and ^{12}C(α,p) reactions. The two prominent peaks observed in Fig. 3(a) find their origin in kinematic constraints which focus both the forward- and backward-emitted particles in the center-of-mass system inside $\approx 25°$ in the laboratory system. Due to the relatively poor energy resolution for these heavy, low-energy fragments, as well as kinematic broadening, it was not possible to distinguish between the (α,n) and (α,p) products or to identify discrete excited $A=15$ states in these studies.

The evolution of the fragment energy spectra with beam energy is shown in Fig. 5 for $A=11$. At the lowest beam energy the distribution is very flat with a rapid falloff in the region of discrete states whereas at the highest beam energy the distributions decrease exponentially, with a smooth transition from one extreme to the other. The exponential falloff at 159 MeV is reminiscent of the spectral shapes observed in high energy proton-induced reactions on ^{12}C.[21] At relativistic projectile energies the fragment energy spectra have been interpreted as originating

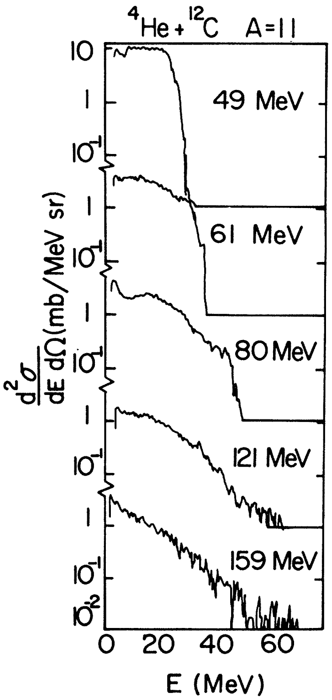

FIG. 5. Energy spectra of fragments with $A=11$ at all beam energies at a laboratory angle of 40 deg.

from a moving hot source. The exponential decrease of the fragment energy spectra may be fitted with a Maxwell-Boltzmann distribution[21] from which the temperature and velocity of the hot source can be deduced. It should be remarked, however, that due to the broad distribution of energy deposition in these reactions (see Sec. III C), the data at 159 MeV represent a high-energy spectral component built upon a composite of all the lower energy spectra. This fact suggests that attempts to extract a common reaction temperature, independent of energy-deposition information, may yield misleading results.

A recent 180-MeV p+^{27}Al experiment[22] shows a similar exponential decrease in all heavy fragment energy spectra. However, attempts at fitting these energy spectra with a single Maxwell-Boltzmann distribution similar to that applied by Westfall *et al.*[21] have been unsatisfactory.

The qualitative features of the energy spectra of fragments obtained in this experiment can be described by a prompt cascade step followed by a statistical Fermi breakup mechanism, as proposed in the accompanying paper.[8] In this model two-body breakup processes dominate the spectra at low beam energies, with the contribution of multibody breakup processes (e.g., ≥ 3) increasing with increasing beam energy. The combined effects of alpha-nucleon and nucleon-nucleon scattering in the cascade step and isotropic multibody fragmentation of highly excited residual fragments in the moving reference frame at the later stages of the interaction are possible mechanisms for fragment production at these intermediate energies. In this model surface effects and the number of particle-stable states of participating fragments play a major role in reproducing the experimental distributions.

B. Angular distributions

Representative laboratory angular distributions for fragments with $A=6$–14 (except $A=8$) are shown in Figs. 6 and 7 for bombardments at 49 and 159 MeV, respectively. The data betweeen these two extremes evolve systematically as a function of bombarding energy, consistent with the behavior of the energy distribution for a given fragment as a function of angle (Fig. 4) and bombarding energy (Fig. 5).

For the lowest energy case at 49 MeV the angular distributions for the heaviest fragments ($A \geq 13$) are strongly forward peaked, indicative of compound nucleus formation followed by particle evaporation. As the fragment mass decreases, the angular spreading of the yield broadens due to the kinematic effects of multiple particle emission and/or decays involving complex nuclei. For the $A=12$ fragments a strong component is also observed near the recoil angle of ~60 deg, as expected for (α,α') reactions. This effect persists in all the data up to 159 MeV. (Note that elastic ^{12}C recoil nuclei are not included in the cross-section analysis.) Increasing the bombarding energy has the effect of spreading the yield to more backward laboratory angles, leading to rather flat angular distributions at forward angles which then fall off exponentially at larger angles. It is a general feature of the data that the slope of the more backward angle data becomes increasingly flat at the higher energies. This is presumably associated with the increase in forward-focused light ions from projectile fragmentation and absorptive breakup

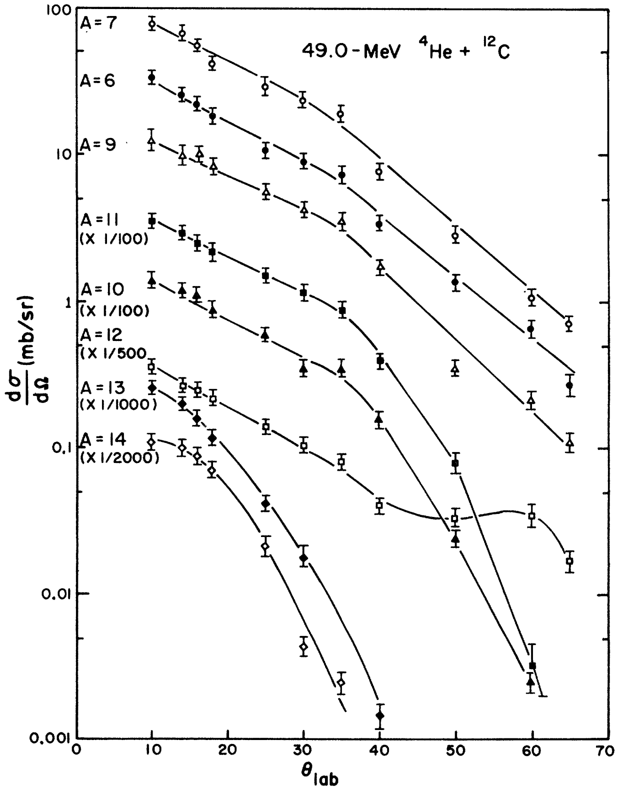

FIG. 6. Laboratory angular distributions for fragments with $A=6$, 7, and 9–14 from the $\alpha+{}^{12}$C reaction measured at 49 MeV. Lines are to guide the eye.

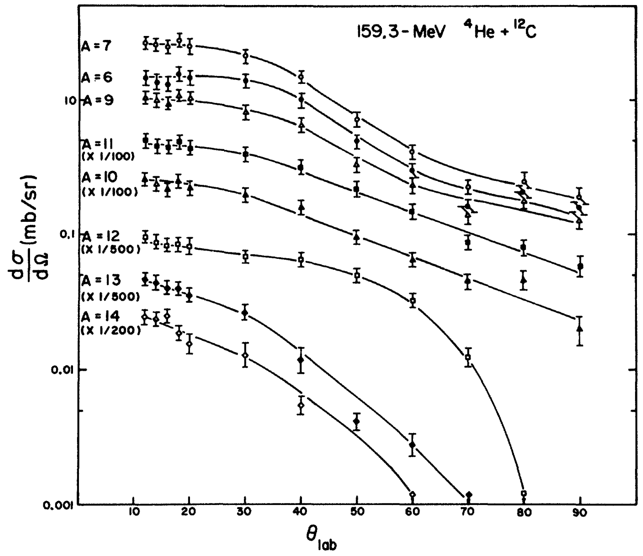

FIG. 7. Laboratory angular distributions for fragments with $A=6$, 7, and 9–14 from the $\alpha+{}^{12}C$ reaction measured at 159 MeV. Lines are to guide the eye.

processes at the higher energies.

As is apparent from the energy spectra in Figs. 3—5, the angular distributions are dominated by multiparticle final states. Analysis of the two-body discrete-state angular distributions also supports the transition in reaction mechanisms discussed above. In Fig. 8 the center-of-mass angular distributions of complimentary fragments from the $^{12}C(\alpha,{}^7Be)^9Be$ and $^{12}C(\alpha,{}^7Li)^9B$ ground-state reactions at 49 and 80 MeV are shown. At 49 MeV the angular distribution of the complementary fragments with $A=7$ and 9 is approximately symmetric about 90 deg, and follows a $1/\sin\theta$ dependence, features characteristic of decay from a compound nucleus. Comparing total and differential cross sections of fragment pairs lighter than the target (e.g., $A=6,10$ and 7,9) with a standard statistical model, Rudy *et al.*[23] have previously shown that compound nucleus decay is the main contributor to the formation of these two-body states. The angular distribution of two-body states from $A=7$ and 9 fragments in our measurements at 49 MeV and those of Rudy *et al.* at 42 MeV (Ref. 23) are in good agreement, both in magnitude and shape. However, as the beam energy increases to 80 MeV (Fig. 8), the angular distributions for these two-body states become increasingly forward peaked, a result indicative of enhanced probability for direct processes. Above this energy the relative importance of two-body states becomes small, as demonstrated in Fig. 9.

The angular distributions of two-body states in which one of the fragments is heavier than the target can result from either stripping reactions or complete fusion followed by statistical decay. The combined angular distribution of the ground states of ^{15}O and ^{15}N from the 80-MeV reaction is shown in Fig. 10. The points beyond 100 deg center-of-mass angle come from the less energetic of the two ground-state peaks (see Fig. 3). The solid line in Fig. 10 was obtained from a zero-range DWBA calculation[24] using optical model parameters from 42-MeV alpha-particle-induced reactions.[25] The real part of the optical potential has been adjusted for 80-MeV particles.

The agreement between experimental and theoretical angular distributions implies that at higher energies the

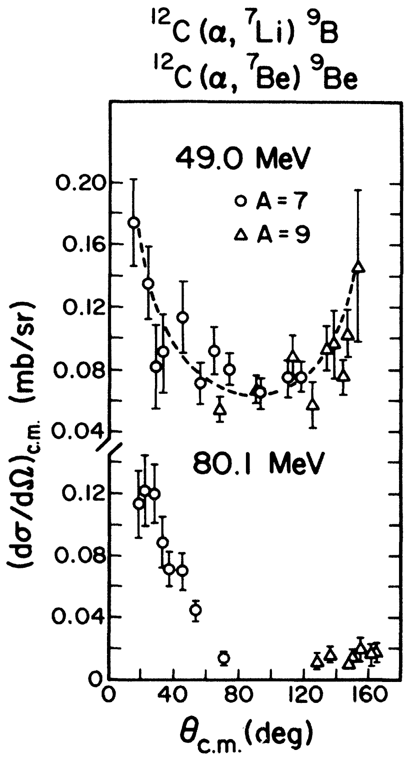

FIG. 8. Center-of-mass angular distribution for the two-body ground-state reactions $^{12}C(\alpha,{}^7Li)^9B$ and $^{12}C(\alpha,{}^7Be)^9Be$ at 49 and 80 MeV. Dashed curve is a $1/\sin\theta$ fit to the data.

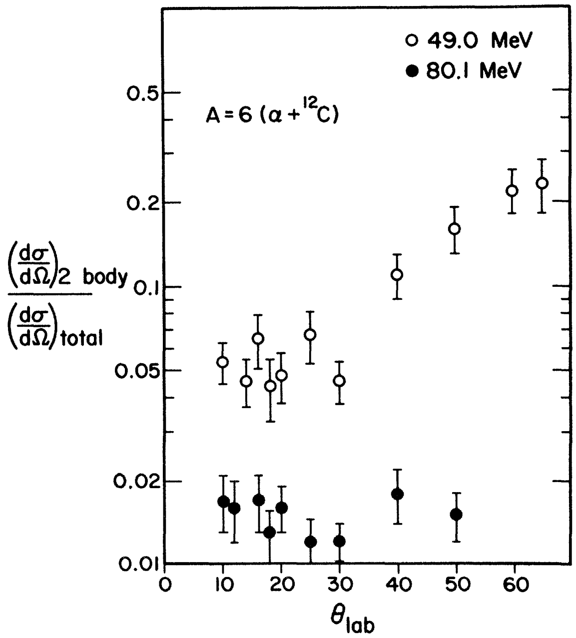

FIG. 9. Ratios of the two-body ground-state cross section to the total isobaric cross section as a function of laboratory angle for $A=6$ fragments from the $^4He+{}^{12}C$ reaction at 49 and 80 MeV.

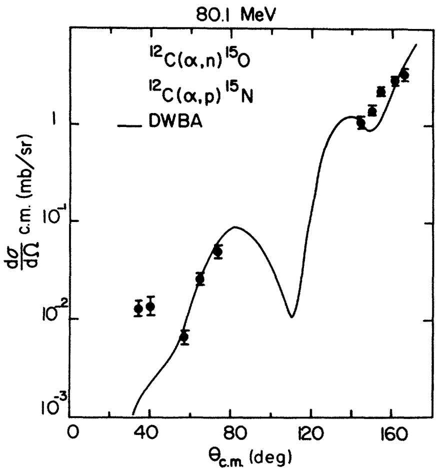

FIG. 10. Angular distributions for combined ^{12}C(α,n)^{15}O and ^{12}C(α,p)^{15}N reactions at 80 MeV. The solid curve is a DWBA calculation, as described in text.

residual nuclei heavier than the target nuclei and their complementary light fragments (e.g., $A<4$) are mainly formed from direct reactions. The mechanisms of ^{12}C(α,n)^{15}O and ^{12}C(α,p)^{15}N reactions have also been studied at 40 MeV.[26,27] The analysis of the angular distributions of neutron and proton spectra by zero-range DWBA calculation suggests that these fragments also originate from direct reactions.

C. Fragment isobaric yields

The isobaric cross sections, obtained from integrating the differential cross sections, are listed in Table I for all incident alpha-particle energies and plotted in Fig. 11. The cross sections for $A=6$, 8, and 9 may not be complete due to decay of the particle-unstable nuclei ^{6}Be, ^{8}Be, and ^{9}B into protons and alpha particles. The major cross section lost is that of ^{8}Be which is a product of the (α,2α) reaction.

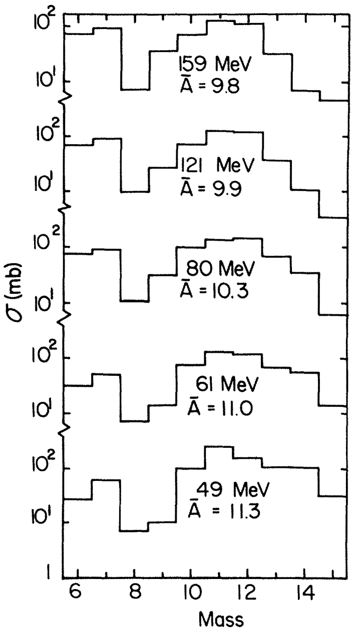

FIG. 11. Mass distributions of all fragments with $A\geq 6$ for the ^{4}He+^{12}C reaction at 49-, 61-, 80-, 121-, and 159-MeV laboratory energy. The average mass, $\bar{A}$, is also indicated for each mass distribution.

At all energies the largest cross sections observed belong to fragments with $A=11$ and 12. The angular distributions in Figs. 6 and 7 suggest that inelastic scattering of alpha particles in the collision stage, leading to excited residuals from (α,α') and (α,α'n) reactions, is a significant contributor to these cross sections. In general, the yields of $A=10$, 11, and 12 vary little over the entire beam energy range. The major changes in the mass distribution as a function of beam energy occur for fragments heavier and considerably lighter than the target nucleus. As the beam energy increases, the cross sections of fragments $A=6$, 7, and 9 increase, whereas those of $A=13$, 14, and 15 systematically decrease.

The mean mass, $\bar{A}$, for each yield curve is also shown

TABLE I. Isobaric and total reaction cross sections (mb).

Mass number	^{4}He+^{12}C Beam energy (MeV) 49.0	61.1	80.1	121.0	159.3
6	26.7± 4.0	31.5± 4.8	76.2±12.5	68.7±13.5	74.8±11.8
7	60.1± 9.1	51.7± 7.8	86.6±13.0	88.0±15.0	95.5±14.3
8	7.2± 1.2	7.0± 1.2	10.0± 2.0	9.8± 2	7.2± 1.1
9	10.1± 1.8	13.9± 2.4	31.3± 3.3	26.9± 5.6	36.0± 5.8
10	97.7±11.2	74.2± 8.7	97.2±14.5	72.0±12.5	75.1±12.3
11	247 ±28	130 ±15	137 ±47	128 ±22	132 ±19
12	154 ±20	119 ±13	147 ±19	122 ±18	117 ±19
13	104 ±12	69 ± 8	68 ± 8	37 ± 5	33 ± 5
14	101 ±11	55 ± 6	35 ± 4	11 ± 2	7.1± 1.3
15	30.6± 3.6	14 ± 2	6.2± 0.8	3.5± 0.6	4.6± 0.8
σ(total)	838 ±41	565 ±26	694 ±57	567 ±38	582 ±34
σ(total)[a]	889 ±67	632 ±60	803 ±85	641 ±64	645 ±62

[a] Data corrected for particle-unstable events due to ^{9}B, ^{8}Be, and ^{6}Be decay.

in Fig. 11. The decrease in $\bar{A}$ with increasing beam energy is consistent with increased energy deposition in the collision stage. However, the rate at which $\bar{A}$ decreases is significantly less than expected for complete fusion of target and projectile. A recent study of linear momentum transfer from light projectiles (e.g., protons, deuterons, and α particles) on heavy target nuclei[28] (e.g., Th and U) has shown that the average linear momentum transfer for ^{4}He projectiles increases with beam energy, reaches a maximum value in the 30—50 MeV/nucleon range, and then decreases at higher energies. The mean value of the mass distributions shown in Fig. 11 appears to saturate as the beam energy approaches ~120 MeV (30 MeV/nucleon). This transition may be associated with the fact that in this energy regime the Fermi velocity of nucleons in the nucleus is comparable to that of projectile velocity, thus permitting nucleon-nucleon interactions to assume greater importance relative to mean field processes.[28]

The excitation functions for each fragment with $6 \leq A \leq 11$ are shown in Fig. 12. The energy range of the available data on excitation functions of fragments with $6 \leq A \leq 11$ from $\alpha + ^{12}$C reactions extends from the reaction threshold to projectile energies in the order of a few GeV.[23,29—36] The low-energy region of the excitation functions is defined by the measurements of Rudy *et al.*[23] who employed a TOF technique for mass identification. Other reaction cross section measurements near the threshold energies by Vidal-Quadras and Ortega[36] used the nuclear emulsion technique.

The excitation functions rise sharply following the thresholds, peak in the energy range of 40—80 MeV (e.g., about 5—10 MeV/nucleon above the reaction threshold), then decrease to a constant limiting value at higher projectile energies. The shape and the location of the peak in the excitation functions for fragments from the ^{4}He$+^{12}$C reaction are similar to those from the p$+^{12}$C and p$+^{16}$O reactions.[18,37] The high-energy tails of the excitation functions of the fragments from this reaction have been estimated from the systematic behavior of these proton-induced reactions. The excitation functions of heavy fragments with $A > 11$ fall off more sharply with projectile energy than those for the lighter fragments in our experimental energy range (Table I). The maxima of the $A > 11$ excitation functions are at lower energies than the lowest beam energy in these measurements so that the threshold region is not well defined. Hence, no excitation functions are plotted for those fragments which are heavier than $A = 11$.

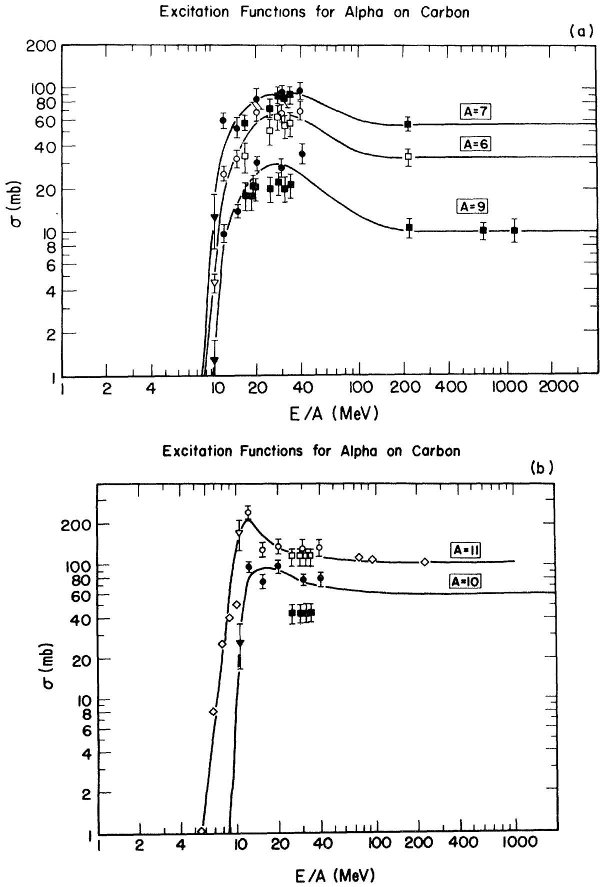

FIG. 12. Excitation functions for fragments with $6 \leq A \leq 11$ from the ^{4}He$+^{12}$C reaction. Data are from this work (○); Ref. 23 (▽); Refs. 29, 31, 34, and 35 (□); and Ref. 33 (◇). Lines are drawn to guide the eye; open and closed symbols serve to differentiate masses.

D. Total reaction cross sections

From the sum of fragment cross sections for $A \geq 6$, total reaction cross sections (σ_R) have been obtained for each beam energy studied here. These are tabulated in Table I. The accuracy of these cross sections obviously depends on the assumption that only one fragment with $A = 6$—15 is produced for each nonelastic event. Two-body states coming from fragments with $A = 6,10$ and 7,9 pairs will contribute twice to the total cross section. However, the well-defined two-body states of these fragments constitute only a small fraction of total cross section (e.g., less than 1%). On the other hand, total disintegration of the target-projectile system into fragments lighter than $A = 6$ results in an underestimate of the cross section. This effect becomes more important as the beam energy increases. In order to determine the degree of complete fragmentation into H and He, the multiplicity of these light particles (e.g., $A \leq 4$) must be measured, which was not done in these studies.

The missing cross sections of isobars $A = 6$, 8, and 9 due to particle-unstable fragments ^{6}Be, ^{8}Be, and ^{9}B have been estimated from the neighboring fragment cross sections assuming a smooth mass distribution and are included as additional entries to σ_R in Table I. Only ^{8}Be constitutes a significant modification to σ_R. These reaction cross sections are compared with the results of two other techniques in Fig. 13. One determination is from the elastic scattering cross section data using optical model fits,[9] and the other is from measurements of flux lost from the beam due to nuclear reactions in passing through a target.[10] The total reaction cross sections obtained are compared with calculations of nucleus-nucleus total reaction cross sections by DeVries and co-workers[9,10] in Fig. 13. Our data points at 49, 80, 121, and 159 MeV are in general agreement with the calculations and the other data.

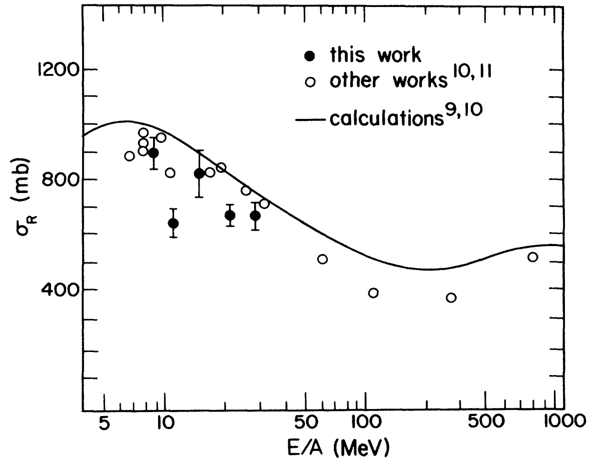

FIG. 13. Total reaction cross sections for the $^4He+^{12}C$ reaction as a function of bombarding energy. Solid circles are from this work; open circles are from Refs. 9 and 10. Solid line is a calculated result from Refs. 9 and 10.

However, the 61-MeV point is significantly lower than the others, which suggests a possible error in the measured target thickness at this energy. The decrease in the total reaction cross section with increasing beam energy can be interpreted as evidence for the increasing influence of nucleon-nucleon collision processes on the interaction mechanism of nucleus-nucleus collisions as a function of energy. This is consistent with the well-known decrease in nucleon-nucleon scattering cross sections as a function of energy.[38]

E. Astrophysical implications

The measured excitation functions for fragments with $6 \leq A \leq 11$ from alpha-particle-induced reactions with ^{12}C, ^{14}N, and ^{16}O (CNO) have astrophysical importance for the nucleosynthesis of Li, Be, and B (LiBeB). The interaction of galactic cosmic rays (GCR) with the interstellar medium[39,40] has been suggested as a primary mechanism to explain LiBeB production. These reactions involve energetic collisions of the primary constituents of the universe with one another; i.e., reactions of protons and alpha particles with ^4He, ^{12}C, ^{14}N, and ^{16}O, and the inverse of these reactions.

In order to test spallation mechanisms for LiBeB production it is necessary to know the target-projectile abundances and the excitation functions for all possible reactions of H, He, C, N, and O that can produce LiBeB. The excitation functions for LiBeB spallation fragments from p+CNO and $^4He+^4He$ systems are rather complete over almost the full range of projectile energies.[41,42] However, little systematic data for the ^4He+CNO systems exist. The energy range of the present experiments (e.g., 50—160 MeV for $\alpha+^{12}C$ and 50—80 MeV for $^4He+^{14}N$ and $^4He+^{16}O$) is important because the excitation functions for these reactions peak in the lower energy region of this range and then become essentially independent of energy at higher energies.

Previous tests of the GCR mechanism[15] have successfully reproduced the observed absolute abundances of the light nuclei ^6Li, ^9Be, ^{10}B, and ^{11}B but underproduce ^7Li by about a factor of 10. The calculated GCR $^{11}B/^{10}B$ and $^7Li/^6Li$ isotopic ratios are a factor of 2 and 10 lower than measured cosmic abundance ratios, respectively. Hence, a secondary goal of the present experiments was to determine whether or not more complete ^4He+CNO cross sections could improve the situation with respect to the ^7Li abundance and $^7Li/^6Li$ and $^{11}B/^{10}B$ ratios predicted by the GCR mechanism.[15] The abundances and abundance ratios predicted by the GCR model have recently been recalculated[43] adding these new measurements to the existing measured cross sections in the literature. These are compared with the experimental abundance values[44] in Table II. The calculated absolute abundance values for ^6Li, ^9Be, ^{10}B, and ^{11}B and the $^6Li/^9Be$ and $B/^6Li$ abundance ratios agree well with the experimental values. However, the calculations still predict the ^7Li abundance to be an order of magnitude smaller than the experimental value. The GCR calculated $^{11}B/^{10}B$ remains about half of the experimental ratio, and the $^7Li/^6Li$ ratio is still an order of magnitude lower than the experimental ratio. Hence, it appears that the data base for calculations of LiBeB abundances via the GCR mechanism is complete and it is highly unlikely that further measurements will significantly influence the present results.

IV. CONCLUSIONS

This work represents one of the first detailed studies of heavy fragment production in the 10—40 MeV/nucleon range with complex projectiles in which mass, energy, and angular distributions have been measured simultaneously for all heavy products. The characteristic feature of the energy spectra is the predominance of a broad continuum

TABLE II. Total abundance (relative to Si$=10^6$) and abundance ratios for the light elements produced in interactions between GCR and the interstellar medium (numbers in parentheses are error factors).

	^6Li	^7Li	^9Be	^{10}B	^{11}B
Experiment (Ref. 44)	2.0(1.4)	25 (1.4)	0.38(2)	1.1(3)	4.3(3)
Calculation (Ref. 43)	2.6	3.4	0.43	2.2	5.5
	$^7Li/^6Li$	$^{11}B/^{10}B$	$^6Li/^9Be$	$B/^6Li$	
Experiment (Ref. 44)	12.6±0.2	4.05±0.1	5.3(2.3)	2.6(2.7)	
Calculation (Ref. 43)	1.3	2.6	6.1	2.9	

which signifies a high probability for multibody final states in the colliison stage and/or decay products of highly excited residual nuclei. The fragment energy distributions are broad and flat at the lowest beam energy and gradually transform into an exponentially decreasing distribution at the highest beam energy, resembling reactions induced by relativistic projectiles. At low beam energies, peaks corresponding to two-body breakup processes appear in the energy spectra. However, at higher beam energies the contribution of two-body states originating from complementary fragments lighter than the target (e.g., $A=6,10$ and 7,9) disappear.

Similarly, the angular distributions of the heavy ($A \geq 13$) fragments demonstrate the evolution from compound nucleus processes, characterized by strongly forward-peaked yields, to a more complex superposition of mechanisms which distribute the yield over a much broader range of angles. Among these possible mechanisms are nonequilibrium, (α,α'), and absorptive breakup processes in the entrance channel, as well as statistical evaporation and multiparticle breakup in the decay stage. Assuming that mass loss is directly related to energy deposition, the mass yield data imply that energy deposition and linear momentum transfer saturate near 30—40 MeV/nucleon, consistent with the results observed with ^{4}He ions incident on much heavier targets.[28] Presumably, this saturation is accompanied by the emission of energetic light ions in the collision stage which carry off the missing momentum. Associated with these effects, a decrease in the total reaction cross section with increasing beam energy is also observed, indicating that the target nucleus becomes more transparent to the incident particles.

Thus, the global picture of these reactions that emerges is one of a relatively smooth transition from mean-field, compound-nucleus-type processes at low energies to complex events at higher energies which emphasize both the nucleon-nucleon aspects of the target-projectile interaction as well as multifragment breakup of highly excited residual nuclei. Reference 8 examines the success of an intranuclear cascade/multifragment breakup model in attempting to account for these data.

Finally, the ^{4}He+CNO reactions are also astrophysically important in explaining LiBeB nucleosynthesis. The addition of these new cross sections to the data base for calculations does not affect the previous conclusions. Hence, now that all the salient reaction cross sections have been measured (p+CNO, ^{4}He+CNO, and ^{4}He+^{4}He), one is left with the conclusion that the GCR mechanism still accounts for ^{6}Li, ^{9}Be, ^{10}B, and ^{11}B relatively well, but underproduces ^{7}Li by approximately an order of magnitude. Thus, the conclusion remains that an additional astrophysical source is required for ^{7}Li synthesis,[15,41] presumably the Big Bang.

ACKNOWLEDGMENTS

We would like to thank Dr. D. A. Goldberg and the University of Maryland Cyclotron staff for providing excellent beams during our experiments. Our special thanks are due to Dr. N. R. Yoder for his help in developing appropriate data analysis codes. We also wish to thank the University of Maryland Computer Science Center for its generous donation of computer time. One of us (A.G.) is grateful to the Turkish Scientific and Technical Research Center for supporting him with a NATO Scholarship during his graduate studies and to the Gillette Company for sponsoring the Gillette Fellowship which provided financial support during the last semester in graduate school. This work was supported by the National Science Foundation and the U. S. Department of Energy.

---

[*] Present address: Middle Eastern Technical University, Ankara, Turkey.

[†] Present address: U.S. Naval Research Laboratory, Washington, D.C. 20375.

[1] D. K. Scott, Nucl. Phys. A354, 375 (1981).

[2] N. S. Wall and P. G. Roos, Phys. Rev. 150, 811 (1966).

[3] F. E. Bertrand and R. W. Peele, Phys. Rev. C 8, 1045 (1973).

[4] C. C. Chang, N. S. Wall, and Z. Fraenkel, Phys. Rev. Lett. 33, 1493 (1974).

[5] J. R. Wu, C. C. Chang, and H. D. Holmgren, Phys. Rev. C 19, 659 (1979).

[6] P. P. Singh, M. Sadler, A. Nadasen, L. A. Beach, and C. R. Gossett, Phys. Rev. C 14, 1655 (1976).

[7] M. D. Glascock, W. F. Hornyak, C. C. Chang, and R. J. Quickle, Phys. Rev. C 19, 1577 (1979); W. F. Hornyak, M. D. Glascock, C. C. Chang, and J. R. Wu, *ibid.* 19, 1595 (1979).

[8] A. Gökmen, G. J. Mathews, and V. E. Viola, Jr., Phys. Rev. C 29, 1606 (1984), the following paper.

[9] R. M. DeVries and J. C. Peng, Phys. Rev. Lett. 43, 1373 (1979).

[10] R. M. DeVries and J. C. Peng, Phys. Rev. C 22, 1055 (1980).

[11] P. U. Renberg, D. F. Measday, M. Pepin, P. Schwaller, B. Favier, and R. Richard-Serre, Nucl. Phys. A183, 81 (1972).

[12] H. A. Bethe, Phys. Rev. 57, 1125 (1940).

[13] N. J. Giacomo, R. M. DeVries, and J. C. Peng, Phys. Rev. Lett. 45, 527 (1980).

[14] H. Nishioka and R. C. Johnson, Phys. Rev. C 22, 2457 (1980).

[15] Sam M. Austin, Prog. Part. Nucl. Phys. 7, 1 (1981).

[16] A. Gökmen, Ph.D. thesis, University of Maryland, 1981.

[17] G. Gabor, W. Schimmerling, D. Greiner, D. Lindstrom, and F. Beiser, Nucl. Instrum. Methods 130, 65 (1975).

[18] R. A. Moyle, B. G. Glagola, G. J. Mathews, and V. E. Viola, Jr., Phys. Rev. C 19, 631 (1979).

[19] N. R. Yoder, Event processor code GEVFPID, University of Maryland Cyclotron Laboratory, 1980.

[20] L. C. Northcliffe and R. F. Schilling, Nucl. Data A7, 233 (1970).

[21] G. D. Westfall, R. G. Sextro, A. M. Poskanzer, A. M. Zebelman, G. W. Butler, and E. K. Hyde, Phys. Rev. C 17, 1368 (1978).

[22] K. Kwiatkowski, S. Zhou, T. E. Ward, V. E. Viola, Jr., H. Breuer, A. Gökmen, A. C. Mignerey, and G. J. Mathews, Phys. Rev. Lett. 50, 1648 (1983).

[23] C. Rudy, R. Vandenbosch, P. Russo, and W. J. Braitwaite, Nucl. Phys. A188, 430 (1972).

[24] D. J. Overway and W. C. Parkinson, Nucl. Phys. A363, 93

(1981).

[25] C. M. Perey and F. G. Perey, At. Data Nucl. Data Tables 17, 1 (1976).

[26] K. van der Borg, R. J. DeMeijer, A. van der Woude, and H. T. Fortune, Phys. Lett. 84B, 51 (1979).

[27] K. van der Borg, R. J. DeMeijer, and A. van der Woude, Nucl. Phys. A273, 172 (1976).

[28] F. Saint Laurent, M. Conjeaud, R. Dayras, S. Haras, H. Oeschler, and C. Volant, Phys. Lett. 110B, 372 (1982).

[29] P. Fontes, C. Perron, J. Lestrinquex, F. Yiou, and R. Bernas, Nucl. Phys. A165, 405 (1971).

[30] C. Baixeras-Aiquabella, J. M. Jung, C. Jacquot, L. Girardin, and R. Schmitt, Phys. Rev. C 2, 1194 (1970).

[31] M. Jung, C. Jacquot, C. Baixeras-Aiquabella, R. Schmitt, and H. Brown, Phys. Rev. C 1, 435 (1970).

[32] G. M. Raisbeck, J. Lestringuex, and F. Yiou, Phys. Rev. C 6, 685 (1972).

[33] J. R. Radin, A. R. Smith, and N. Little, Phys. Rev. C 9, 1718 (1974); M. Lindner and R. M. Osborne, Phys. Rev. 91, 1501 (1953).

[34] J. Lestringuex, G. M. Raisbeck, F. Yiou, and R. Bernas, Phys. Lett. 36B, 331 (1971).

[35] G. M. Raisbeck and F. Yiou, Phys. Rev. Lett. 35, 155 (1975).

[36] A. Vidal-Quadras and M. Ortega, Nuovo Cimento 49A, 235 (1979).

[37] C. T. Roche, R. G. Clark, G. J. Mathews, and V. E. Viola, Jr., Phys. Rev. C 4, 410 (1976).

[38] G. Alkhazov, T. Bauer, R. Bertini, L. Bimbot, O. Bing, A. Boudard, G. Bruge, H. Catz, A. Chaumeaux, P. Couvert, J. M. Fontaine, and F. Hibou, Nucl. Phys. A280, 365 (1977).

[39] H. Reeves, W. A. Fowler, and F. Hoyle, Nature (London) 226, 727 (1970).

[40] M. Meneguzzi, J. Audouze, and H. Reeves, Astron. Astrophys. 15, 337 (1971).

[41] B. G. Glagola, V. E. Viola, Jr., H. Breuer, N. S. Chant, A. Nadasen, P. G. Roos, and S. M. Austin, Phys. Rev. C 25, 34 (1982).

[42] S. M. Read and V. E. Viola, Jr., At. Data Nucl. Data Tables (in press).

[43] T. P. Walker, G. J. Mathews, and V. E. Viola, Jr., Indiana Nuclear Chemistry Report INC-40007-3, 1984.

[44] H. Reeves and J. P. Meyer, Astrophys. J. 226, 613 (1978).